MULTI-PHYSICS AND MULTI-SCALE METHODS FOR MODELING FLUID FLOW THROUGH NATURALLY FRACTURED CARBONATE KARST RESERVOIRS

P. Popov, G. Qin, L. Bi, Y. Efendiev, Institute for Scientific Computation, Texas A&M University; Z. Kang, J. Li, Research Institute of Petroleum Exploration and Development, SINOPEC Corporation, Beijing, P.R. China

Summary

Modeling and numerical simulations of Carbonate Karst reservoirs is a challenging problem due to the presence of vugs and caves which are connected via fracture networks at multiple scales. In this paper we propose a unified approach to this problem by using the Stokes-Brinkman equations which combine both Stokes and Darcy flows. These equations are capable of representing porous media (porous rock) as well as free flow regions (fractures, vugs, caves) in a single system of equations. The Stokes-Brinkman equations also generalize the traditional Darcy-Stokes coupling without sacrificing the modeling rigor. Thus, it allows us to use a single set of equations to represent multiphysics phenomena on multiple scales. The local Stokes-Brinkman equations are used to perform accurate scale-up. We present numerical results for permeable rock matrix populated with elliptical vugs and we consider upscaling to two different coarse-scale grids - 5×5 and 10×10. Both constant and variable background permeability matrices are considered and the effect the vugs have on the overall permeability is evaluated. The Stokes-Brinkman equations are also used to study several vug/cave configurations which are typical of Tahe oilfield in China.

Introduction

Naturally fractured karst reservoirs presents multiple challenges for numerical simulations of various fluid flow problems. Such reservoirs are characterized by the presence of fractures, vugs and caves at multiple scales. Each individual scale is an ensemble of porous media, with well defined properties (porosity and permeability) and a free flow region, where the fluid (oil, water, gas) meets no resistance form the surrounding rock [1].

The main difficulty in numerical simulations in such reservoirs is the co-existence of porous and free flow regions, typically at several scales. The presence of individual voids such as vugs and caves in a surrounding porous media can significantly alter the effective permeability of the media. Furthermore, fractures and long range caves can form various types of connected networks which change the effective permeability of the media by orders of magnitudes. An additional factor which complicates the numerical modeling of such systems is the lack of precise knowledge on the exact position of the interface between the porous media (rock) and the and vugs/caves. Finally, the effects of cave/fracture fill in by loose material (sand, mud, gravel, etc), the presence of damage at the interface between porous media and vugs/caves and the roughness of fractures can play very important role in the overall response of the reservoir.

The modeling of fractured, vuggy media is traditionally done by using the coupled Stokes-Darcy equations [1, 2, 3, 4, 5, 6, 7, 8, 9, 10, 11]. The porous regions is modeled by the Darcy equation [4, 12], while the Stokes equation is used in the free flow region. At the interface between the two, various types of interface conditions are postulated [2, 3, 4, 5]. All of these interface conditions require continuity of mass and momentum across the interface. The difference comes when the tangential component of the velocities at the interface are treated. Each one of them proposes a different jump condition for the tangential velocities and/or stresses, related in some way to the fluid stress. The selection of jump condition is subject to the fine structure of the interface and the flow type and regime (c.f. e.g. [13] and the references therein). Furthermore, these jump conditions introduce additional media parameters that need to be determined. These parameters can be obtained either experimentally, or computationally.

There are several aspects of the coupled Darcy-Stokes approach, which make its application to vuggy reservoirs complicated. First, good knowledge is required both in the location of the porous/fluid interface as well as its fine-scale structure. Such precise information is hard to deduce from subsurface geological data. Secondly, there is need to obtain, numerically or experimentally values for parameters related to the interface conditions. Numerical determination is viable for engineered media, such as oil filters in the automotive industry, where the fine-scale porous geometry is known, either by design or can be obtained relatively easily, for example by 3D tomography. The experimental approach is more appropriate for subsurface formations, however, there are many difficulties associated with it. Finally, the free flow region which represents caves/vugs and fractures must be free of any obstacles such as loose fill-in material, and the fluid must also be free of any particle suspensions which are moving with it.

An alternative way of modeling vuggy media is to use the Stokes-Brinkman equations [1, 13, 14, 15, 16, 17, 18, 19]. These equations provide a unified approach in the sense that a single equation with variable coefficients is used for both porous and free-flow region. Stokes-Brinkman equations can be reduced to Stokes or Darcy equations by appropriate choice of the parameters. Since the different media types are distinguished by selecting the coefficients of the partial differential equation, there is usually no need to formulate specific interface conditions.

This is especially helpful in reservoir and groundwater flow, where the porous domain has a complicated topology. The numerical treatment of Stokes-Brinkman equation is simpler, due the lack of special interface conditions. Also, due to uncertainties associated with interface locations between vugs and the rock matrix, Stokes-Brinkman equations introduce a somewhat coarse model that does not require precise interface locations and avoid local grid refinement issues that are needed near the interfaces. Finally the Stokes-Brinkman equations provide a model that can be continuously varied from a Darcy dominated flow to a Stokes dominated flow, a feature which allows is to simulate effectively partially filled fractures or solid particles suspended in the fluid.

The two mathematical models for the fine scale: the Stokes-Darcy and the alternative proposed in this work, the Stokes-Brinkman model, are presented next. This is followed by a short discussion on the upscaling of the Stokes-Brinkman equation from the fine to the coarse scale. Two different types of numerical examples are presented. The first demonstrates that upscaling the Stokes-Brinkman model works for isolated vugs distributed in a porous matrix. The effect of upscaling resolution is also investigated. The second class of examples deal with several typical configurations in a carbonate karst reservoir in China.

Mathematical Models for Vuggy Media at Multiple Scales

We begin, by considering two scales, a fine and a coarse one. The fine scale media is composed of a porous region and a free flow region. The free flow region represents the vugs, caves and fractures. The porous region, which we will also refer to as matrix, has a much finer underlying structure of impermeable solid and pore space where fluid flow can occur. This fine scale structure is not considered but an effective response of the porous media is assumed governed by material parameters such as porosity and permeability.

At the coarse scale, on the other hand, the media is described mostly by Darcy flow. The fine scale features such as vugs caves and fractures, along with the surrounding porous matrix, are replaced by an effective material with well defined effective permeability and porosity. However certain features, such as, large, long-range caves (relative to the fine scale) may still be retained at the coarse scale. In the later situation, the Stokes-Brinkman model provides a very natural way of transiting between the scales.

To fix notation, the characteristic length scales of the fine and coarse scale, are denoted by l and L, respectively. Next, the usual small parameter ε is introduced [6, 20]:

$$\varepsilon = \frac{l}{L}. \tag{1}$$

Throughout this section, all quantities with superscript ε are defined on the fine scale, otherwise they are defined on the coarse scale. Let Ω^f be the free flow region, Ω^p the porous region and the interface between the two (excluding the external boundary) be Γ. Also, the fine scale fluid velocity is denoted by $\mathbf{v}^\varepsilon$ and the fine scale pressure by p^ε. In the free flow region, $\mathbf{v}^\varepsilon$ represents the actual physical velocity of the fluid but in the porous region it represents the Darcy (or averaged) velocity.

Darcy-Stokes The Stokes equation, used to describe the free flow region, has the form:

$$\nabla p^\varepsilon - \mu \Delta \mathbf{v}^\varepsilon = \mathbf{f} \qquad \text{in } \Omega^f, \tag{2}$$

$$\nabla \cdot \mathbf{v}^\varepsilon = 0 \qquad \text{in } \Omega^f. \tag{3}$$

The first of these equation expresses the balance of linear momentum, and the second is the conservation of mass. Also, recall the fluid stress tensor $\boldsymbol{\sigma}$ is given by the formula:

$$\boldsymbol{\sigma} = -p\mathbf{I} + 2\mu\mathbf{D},$$

where $\mathbf{D}$ is the strain rate:

$$\mathbf{D} = \frac{1}{2}\left(\nabla \mathbf{v} + \nabla \mathbf{v}^T\right).$$

In the porous region, one has the classical Darcy law (c.f. e.g. [12, 6]), along with conservation of mass:

$$\mathbf{v}^\varepsilon = -\frac{\mathbf{K}}{\mu}\left(\nabla p^\varepsilon - \mathbf{f}\right) \qquad \text{in } \Omega^p, \tag{4}$$

$$\nabla \cdot \mathbf{v}^\varepsilon = 0 \qquad \text{in } \Omega^p. \tag{5}$$

The two systems need to be coupled at the interface Γ. There are various ways in which this is achieved. For example, the classical condition of [2] states that:

$$[\mathbf{v}] \cdot \mathbf{n} = 0 \qquad \text{on } \Gamma, \tag{6}$$

$$2\mu \mathbf{D}\mathbf{n} = [p] \qquad \text{on } \Gamma, \tag{7}$$

$$\frac{\partial \mathbf{v}_f}{\partial \mathbf{n}} = \frac{\alpha_{BJ}}{\sqrt{K}}[\mathbf{v}] \cdot \mathbf{t}_i \qquad \text{on } \Gamma. \tag{8}$$

Here, $[\cdot]$ denotes the jump in a given quantity while moving from the fluid to the porous side, that is, form some field ϕ:

$$[\phi] = \phi_f - \phi_p,$$

$\mathbf{n}$ is a unit normal pointing from Ω^f to Ω^p and $\mathbf{v}_f$ is the velocity in the fluid region. In the above equations, the first interface condition (6) expresses conservation of mass across the interface, (7) expresses conservation of momentum, and (8) imposes a slip condition on the tangential component of the velocity. The dimensionless constant α_{BJ} is a material property which is representative of the microstructure (at much smaller scales than l) of the interface. It can be obtained either numerically, if such information is available or obtained experimentally.

It should be emphasized, that the exact form of the interface conditions (6)-(8) is an active area of research [2, 3, 4, 5, 8, 9, 10]. For example, [3] modified equation (8) to contain only variable in the fluid domain, [4, 5] studied

the interface conditions based on the flow type, e.g. parallel or perpendicular to the interface [4, 5] and [8, 9, 10] studied the mathematical justifications of such interface conditions. The reader is referred to [13] for a detailed review.

The Stokes-Brinkman Equation Recall that the fine scale velocity is denoted by $\mathbf{v}^\varepsilon$ and the fine scale pressure by p^ε. The Stokes-Brinkman equation for a single phase flow in a porous/free flow media is written as follows (c.f. e.g. [14, 13]):

$$\mu \mathbf{K}^{-1}\mathbf{v}^\varepsilon + \nabla p^\varepsilon - \mu^* \Delta \mathbf{v}^\varepsilon = \mathbf{f} \qquad \text{in } \Omega, \tag{9}$$

$$\nabla \cdot \mathbf{v}^\varepsilon = 0 \qquad \text{in } \Omega. \tag{10}$$

Here, $\mathbf{K}$ is a permeability tensor, which in Ω^p is equal to the Darcy permeability of the porous media, μ is the physical viscosity of the fluid and μ^* is an effective viscosity. The other two parameters - $\mathbf{K}$ and μ^* are selected differently depending on the media type (porous or free flow) and are discussed next. It will also be shown that, in the fluid region, $\mathbf{v}^\varepsilon$ represents the actual physical velocity of the fluid and in the porous region, it is the Darcy velocity.

The physical fluid viscosity μ is a material constant that defines the fluid under consideration (e.g. water, oil, etc) and is a uniform constant in the entire domain Ω. In the fluid region Ω^f, $\mathbf{K}$ is assumed to be ∞ and μ^* is taken equal to the physical fluid viscosity μ:

$$\mu^* = \mu, \qquad \mathbf{K} = \infty \qquad \text{in } \Omega^f \tag{11}$$

Observe that this selection of parameters implies that equations (9), (10) reduce to the Stokes system (2), (3).

In the porous region Ω^p, $\mathbf{K}$ is taken to be the Darcy permeability of the porous media. With that, and in the absence of distributed body force $\mathbf{f}$, equation (9) can be written as

$$\nabla p^\varepsilon = -\mu \mathbf{K}^{-1}\mathbf{v}^\varepsilon + \mu^* \Delta \mathbf{v}^\varepsilon \qquad \text{in } \Omega, \tag{12}$$

The reader will recognize that in the last equation, the only difference with Darcy's law (4) is the additional viscous term $\mu^*\Delta\mathbf{v}^\varepsilon$. So, if μ^* is taken equal to zero in Ω^p, then equation (9) reduces to (4). However this will reduce the Stokes-Brinkman system to the coupled Darcy-Stokes model. This will entail the difficulties mentioned previously, which we aim to avoid. Observe, that in most porous media, $\mathbf{K}$ is in the range of milli- to tens of Darcy. Thus, if μ^* is of the same order as the physical viscosity μ, that is

$$\mu^* \sim \mu$$

the term $\mu\mathbf{K}^{-1}\mathbf{v}^\varepsilon$ in equation (12) dominates by many orders of magnitude $\mu^*\Delta\mathbf{v}^\varepsilon$. Thus, the additional viscous term introduces only a small perturbation to Darcy's law. As a result the simplest possible choice for μ^* is

$$\mu^* = \mu$$

which, in complex geometries, uncertain interface location and lack of knowledge of the micro-scale interface features is a reasonable choice [13, pg. 26-29]. A different choice of μ^* is usually motivated by two factors. First, μ^* can be used to provide a more accurate model for the porous medium than is afforded by Darcy law [15, 17, 19]. Secondly, the effective viscosity μ^* can also be used to mimic various jump condition at the interface, as done by [16, 21]. The reader is again referred to [13, pg. 26-29], for an in-depth discussion on this subject.

The Stokes-Brinkman equation offers several advantages. First, it allows a unified approach to the ensemble of porous and free-flow media by formulating a single equation in the entire domain Ω. The different media types are distinguished by proper selection of $\mathbf{K}$ and μ^* in equations (9), (10) and there is no need to formulate specific interface conditions, as in the coupled Darcy-Stokes approach. This is especially helpful when the porous domain Ω^p has a complicated topology, as is the case in vuggy reservoirs. The unified approach also translates to significant simplification in the numerical treatment of equations (9), (10).

Upscaling As was mentioned earlier, vuggy, fractured reservoirs feature multiple scales, and upscaling is necessary for numerical simulation at the field scale. In this section, we consider the upscaling of the Stokes-Brinkman equation from the fine to the coarse scale.

First, we assume that we have a Representative Element of Volume (REV) which features both porous and fluid domains. In this case, the coarse scale equations are Darcy law and conservation of mass. The short summary presented next is based on two-scale asymptotic expansion [6, 20]. The procedure is very similar to the one employed for upscaling the Stokes equation in an impermeable porous media. The reader is thus referred to [22] for technical details. The results are summarized next. A formal asymptotic expansion of the type

$$\mathbf{v}^\varepsilon(\mathbf{x}) = \mathbf{v}_{-2}(\mathbf{x},\mathbf{y}) + \varepsilon\mathbf{v}_{-1}(\mathbf{x},\mathbf{y}) + \varepsilon^2\mathbf{v}_0(\mathbf{x},\mathbf{y}) + \varepsilon^3\mathbf{v}_1(\mathbf{x},\mathbf{y}) + \dots \tag{13}$$

$$p^\varepsilon(\mathbf{x}) = p_0(\mathbf{x},\mathbf{y}) + \varepsilon p_1(\mathbf{x},\mathbf{y}) + \dots \tag{14}$$

is substituted in equations (9), (10). By further assuming that

$$\mu\mathbf{K}^{-1} \geq \mathcal{O}\left(\varepsilon^{-2}\right), \tag{15}$$

one obtains that the first two velocity terms $\mathbf{v}_{-2}$ and $\mathbf{v}_{-1}$ are identically zero and the first term in the pressure expansion p_0 does not depend on the fine-scale variable $\mathbf{y}$, that is $p_0 = p_0(\mathbf{x})$.

Next, one obtains a set of cell problems that are used to compute the effective (or upscaled) permeability of the REV. Let d be the dimension (2 or 3) and $\mathbf{e}_i$ be a unit vector in the i-th direction. The d cell problems needed to upscale the Stokes-Brinkman equation are:

$$\mathbf{K}^{-1}\mathbf{w}^i + \nabla_{\mathbf{y}} q^i - \frac{\mu^*}{\mu}\Delta_{\mathbf{y}}\mathbf{w}^i = \mathbf{e}_i \qquad \text{in } Y, \tag{16}$$

$$\nabla_{\mathbf{y}} \cdot \mathbf{w} = 0 \qquad \text{in } Y. \tag{17}$$

Here, $\mathbf{w}^i$ are Y-periodic and the (fine-scale) pressure q has zero average in Y. The permeability is then computed by averaging the fine-scale velocities:

$$K_{ij} := \langle {w_i}^j \rangle_Y = \frac{1}{|Y|} \int_Y w_i d\mathbf{y}. \tag{18}$$

The macroscopic (upscaled) flux is given by the Darcy's law:

$$\langle \mathbf{v}^\varepsilon \rangle = -\frac{\mathbf{K}}{\mu} \left(\nabla \langle p^\varepsilon \rangle - \mathbf{f} \right), \tag{19}$$

and subject to conservation of mass:

$$\nabla \cdot \langle \mathbf{v}^\varepsilon \rangle = 0. \tag{20}$$

Note that $\mathbf{w}^i$, $i = 1, ..., d$ are the fine-scale velocities in the REV, that is Y, are subject to unit forcing in the respective direction. Since $\mathbf{e}_i$ can also be transferred to the pressure term:

$$\nabla \left(\mathbf{q}^i + x_i \right) = \nabla \mathbf{q}^i + \mathbf{e}_i,$$

one can consider $\langle \mathbf{w}^i \rangle$ as the averaged flux in Y over a unit pressure drop in the i-th coordinate direction.

The above upscaling works well under the assumption (15) and that an REV consisting of both porous and fluid region exists. Assumption (15) is quite general, since typically $\mathbf{K}^{-1}$ dominates the fluid viscosity by orders of magnitude. When $\mathbf{K} \sim \varepsilon^2 \mu$ the Brinkman term in the porous part of equation (16) is significant. The fine-scale velocities in the porous and fluid region will be of similar orders and noticeable mass transfer will occur between the fluid and solid, regardless of the flow regime. When $\mathbf{K} \ll \varepsilon^2 \mu$, the Brinkman term in (16) will dominate in the porous part of Y. As a result, the flow will significantly depend on the geometry of the REV. For example, in the case of connected vugs, the flow trough the vugs will dominate any flow in the porous part and one will essentially be homogenizing Stokes flow in impermeable media.

It is also possible that the some regions of the fine-scale domain do not allow upscaling, for example when an REV contains only a fluid part. This will happen if there are fluid regions with characteristic size much larger then l, c.f. equation (1). In such cases one can upscale the part of the fine scale where suitable mixture of porous media and vugs exist. Large scale voids on the other hand can be retained as free flow regions at the coarse scale. Then one will have a homogenized Stokes-Brinkman equation on the coarse scale, where the fluid region is represented by vugs, caves or fractures that cannot be homogenize. The porous region is the part susceptible to homogenization. There, the macroscopic velocity and pressure are defined as the average of the respective fine-scale quantities. In this way, the Stokes-Brinkman model allows us to upscale fractured, vuggy media, in a natural way and retaining the same equation at all scales. This allows successive homogenization at multiple scales.

Numerical Experiments

Discretization In order to solve numerically the fine-scale problem (9), (10), as well as the cell problems (16), (17) we use a mixed finite element method for the Stokes-Brinkman equations in the primary variables. We use Taylor-Hood elements (continuous quadratic velocity and continuous linear pressure, for more details, see e.g. [23]) on unstructured grids. The Taylor-Hood element is one of the few commonly used elements for the Stokes equation which is also stable for the Stokes-Brinkman equation [24]. It also provides a good approximation for both velocity and pressure.

The linear systems resulting from this finite element discretization are symmetric and indefinite and are solved using preconditioned conjugate gradient method for the pressure Schur complement. For more details on these types of numerical the reader is referred to [23]. The coarse-scale problems (19), (20) are solved by standard, conforming finite element method (c.f. e.g. [25]).

Influence of the viscous term in the porous regions As was mentioned previously, the viscous term in the porous region introduces a small perturbation to the Darcy flow (c.f. equation (12)). In this section we present a numerical example which demonstrates that this is the case. The geometry is a simple REV, consisting of a porous square with a circular vug in the center. The porous matrix is taken with very high permeability $K = 100D$ and the fluid is water ($\mu = 1cP$). The permeability was chosen intentionally very high so that one could see a noticeable effects of the Brinkman term in the porous region when $\mu^* = \mu$. Periodic boundary conditions are specified for both pressure and velocity. The flow is driven by a unit force in the horizontal direction.

Several simulations were performed, using different values for μ^* in the porous region. In Figure 1(a) the velocity and streamlines are plotted for a single vug inclusion and homogeneous background permeability field using Stokes-Brinkman equations (5) with $\mu^* = \mu$. This natural choice was proposed by Laptev [13] in the absence of good knowledge of the porous-fluid interface microstructure, exact location, etc. Note that the flow is driven by a unit body force. This, combined with the periodic boundary conditions leads to a pressure which is antisymmetric with respect to the line $x = 0.5$. Moreover, it reaches its minimum near the left border of the inclusion (as the fluid enters the free flow region it experiences the least resistance to flow) and maximum at the right end of the inclusion (as the fluid enters back into the porous region the flow experiences higher resistance).

In Figure 1(b), the same quantities are plotted for the solution of the Stokes-Brinkman with much smaller viscosity term in the porous region ($\mu^* = 0.001\mu$). The pressure for the two cases is plotted in Figures 1(c) and 1(d), respectively. Comparing with the case $\mu^* = \mu$, the two solutions are essentially the same, with about 1% change in the maximum value of the velocity. This can be ex-

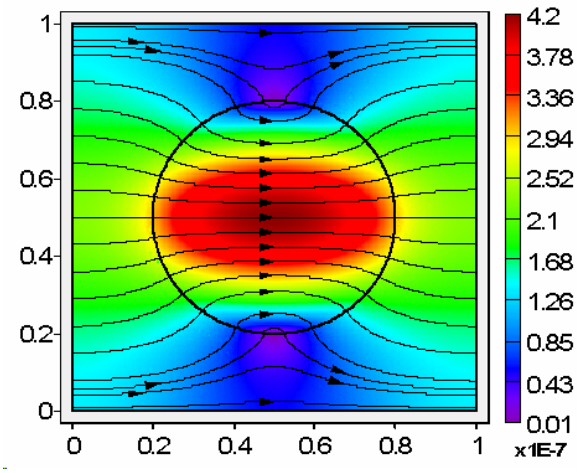

(a) $\mu^* = \mu$, streamlines and velocity magnitude.

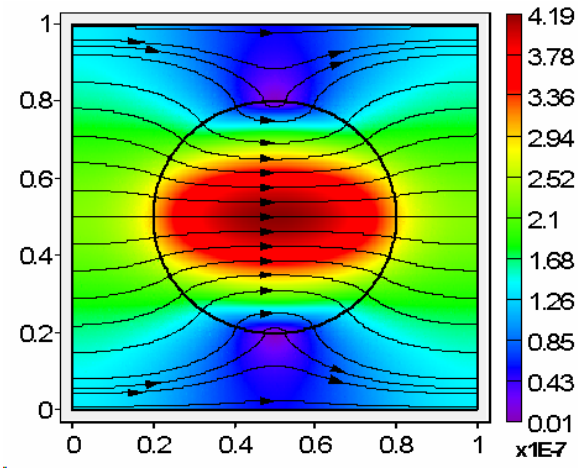

(b) $\mu^* = 0.001\mu$, streamlines and velocity magnitude.

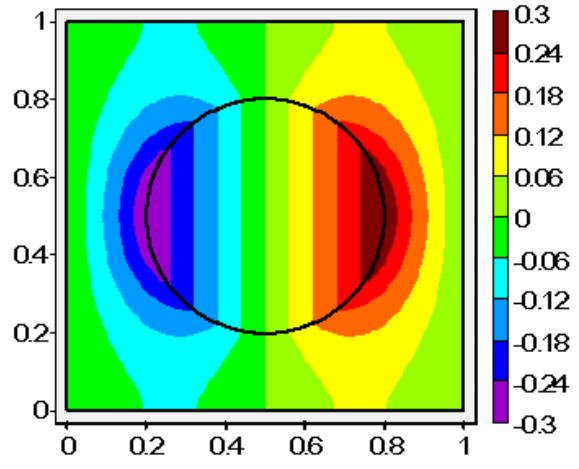

(c) $\mu^* = \mu$, pressure

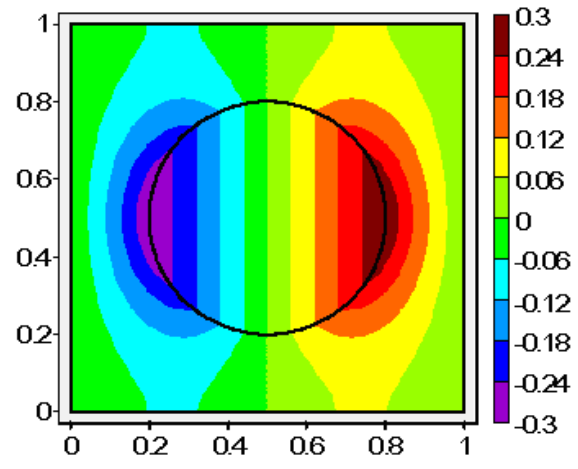

(d) $\mu^* = 0.001\mu$, pressure

Figure 1: Effect of the viscous term in the porous region of the Stokes-Brinkman equation.

plained by observing that even for the very high permeability in the porous region ($100D$), the Brinkman term dominates over the viscous term by seven orders of magnitude: $\mu/K = 10^7$. Further decrease of μ^* in the porous region did not change the velocity field any further. Because there is almost no difference between the velocity and pressure fields, and since in realistic reservoirs there is little hope to obtain detailed information of the porous-fluid interface, all further simulations will be performed with $\mu^* = \mu$.

A 3-Dimensional Example In this section we compute the solution of the Stokes-Brinkman equations in a simple 3D geometry consisting of a porous block with a spherical vug in the center (Figure 2). The block is a cube with unit dimensions ($1m$) and the spherical vug has radius $0.3m$. The porous rock matrix has permeability $K = 100D$ and the fluid under consideration is water. The discretization of the REV domain is performed using tetrahedral Taylor-Hood elements. Due to symmetry, only half of the domain is used (Figure 2(b)).

The boundary value problem considered is one of the three cell problems needed to find the upscaled properties of this REV. That is we impose periodic boundary conditions and a unit body force in the x_1 direction (c.f. equations (16) and (17)). The result indicate that the upscaled permeability K^* of this REV is $137D$. The velocity and pressure profiles of the solution itself are shown in Figure 3.

Upscaling of randomly distributed, disconnected vugs In this section we perform numerical experiments designed to test the upscaling of Stokes-Brinkman equations. We consider a fine scale domain populated with randomly distributed elliptical vugs, shown in Figure 4(a). In the figure, the vugs are colored in red. They are generally well separated from each other and not connected. The objective is to compare a fine scale solution of equations (9), (10) with the coarse scale model (19), (20). We considered two cases depending on the permeability in the porous region. In both cases the fluid under consideration is water ($\mu = 1cP$). In the first case the background permeability was taken homogeneous in order to understand the effect of the vugs. The second example is more realistic. A variable background permeability field is considered (Figure 7(a)). For each example we performed upscaling to a 5×5 coarse grid and a 10×10 coarse grid. This al-

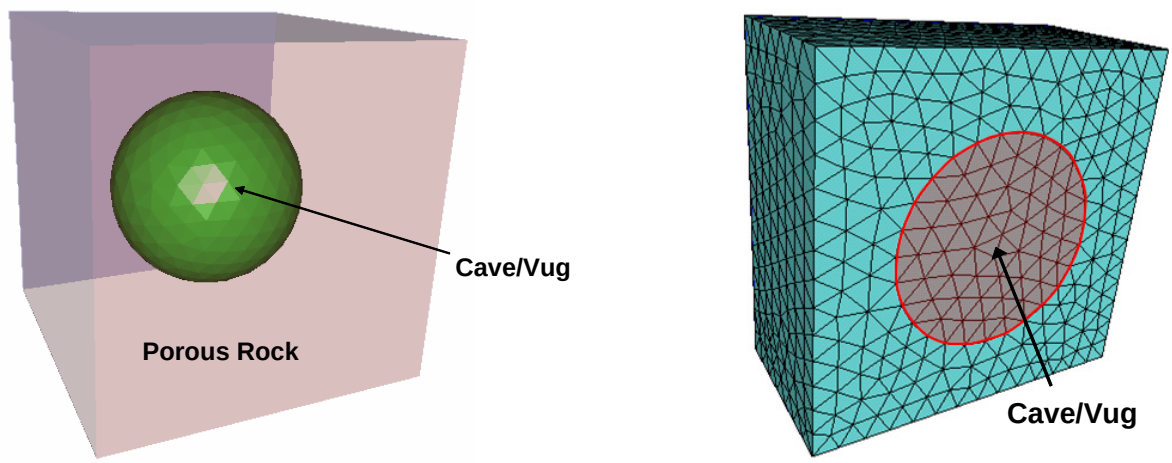

(a) REV Geometry (b) Discretization

Figure 2: A 3D REV (a) consisting of cubic block of porous (transparent) with a spherical vugular inclusion (green) in the center. The unstructured tetrahedral mesh used in the computations is shown to the right (b). Note that due to symmetry only half of the domain is used

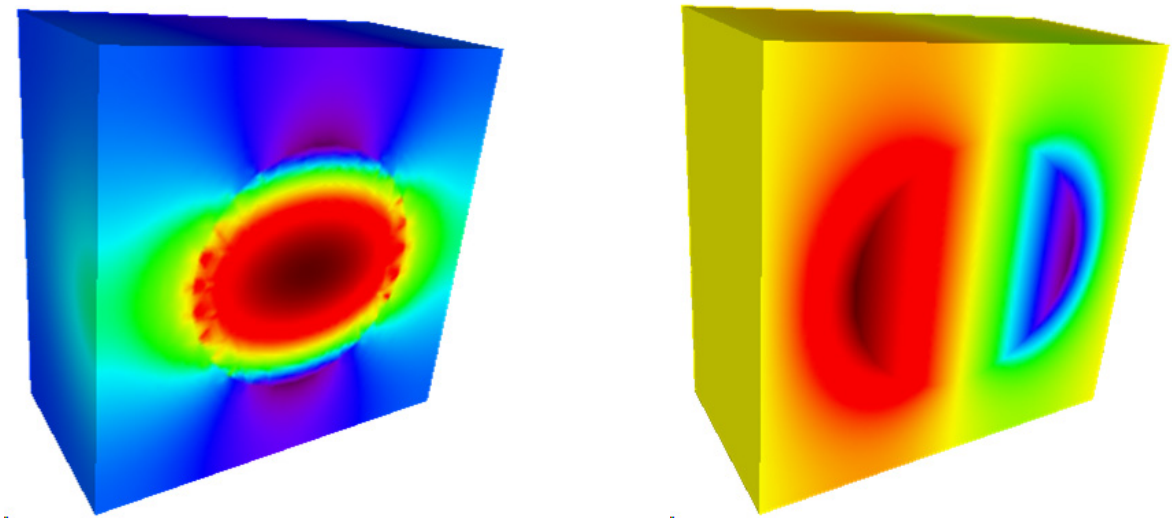

(a) Velocity in the x_1 direction (b) Pressure

Figure 3: REV solution for a 3D spherical inclusion

lowed us to study the quality of the upscaled solution as the coarse grid was refined. Finally, all fine-scale computations were performed on the mesh shown in Figure 4(a) (35272 triangular elements and 17879 nodes).

Homogeneous matrix permeability In the first example, the background permeability field is homogeneous with $K = 1mD$. We consider no flow at top and bottom sides of the domain (Figure 4(a)). The flow is driven by a unit pressure drop in the horizontal (x) direction. This is achieved by setting a $1Pa$ pressure at the left side and zero at the right side of the domain.

The fine scale solution is shown in Figure 4(b) and Figure 4(c). Next we construct two different coarse scale models by dividing the whole domain into 10x10 and 5x5 coarse grid blocks, as shown in Figure 5 and 6. For each coarse grid, the upscaled permeability is computed (c.f. the cell problems (16), (17)). The horizontal and vertical components of the effective permeability tensor K is shown respectively. Observing these figures, we can clearly see that in the coarse regions with high concentration of vugs, the upscaled permeability is higher. Further more, the results from higher coarse scale resolution more accurately represent the distribution of vugs. The corresponding coarse scale pressure solutions are plotted in Figure 5(c) and Figure 6(c). We compare this coarse-scale pressure with the averaged coarse-scale pressure obtained from fine-scale pressure. Table 1 gives the absolute and relative L_2 errors in different cases. The relative L_2 errors of both coarse scale models were found to be less than 2%. The 10x10 case is more accurate than the 5x5 case because higher resolution can better represent the heterogeneous distribution of vugs.

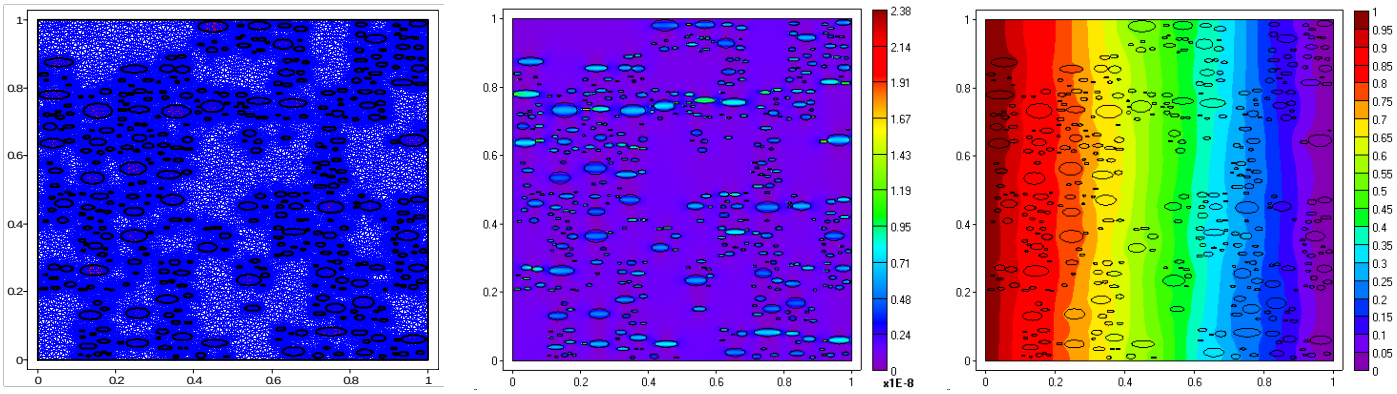

(a) Discretization (b) Velocity magnitude (c) Pressure

Figure 4: Fine-scale geometry (a) and reference solution (b,c) for vugs in homogeneous background permeability field. The fine-scale geometry and finite element discretization are shown in (a) with the vugs colored in red. The fine-scale reference solution is shown in (b) and (c).

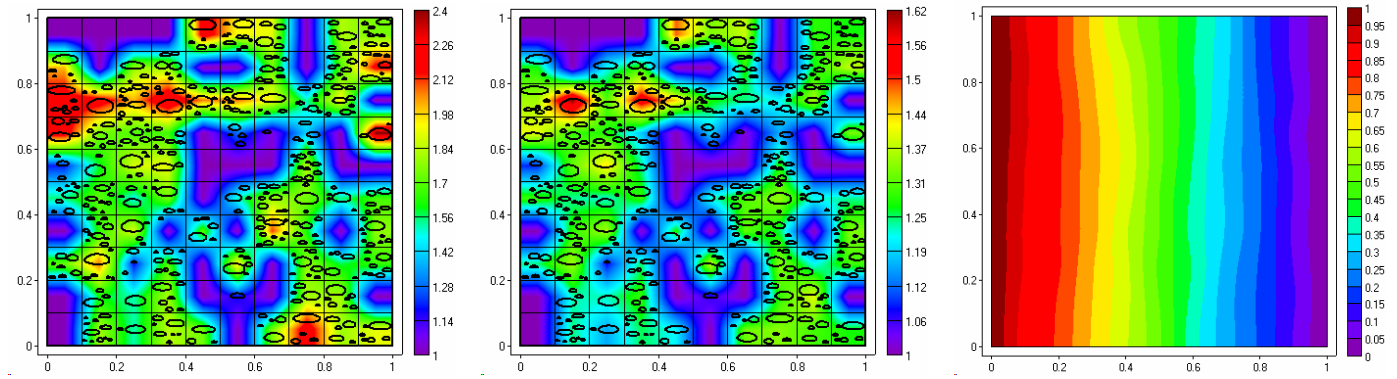

(a) K_{11} (b) K_{22} (c) Coarse-scale pressure

Figure 5: Upscaling results for vugs in homogeneous background permeability field on a 10×10 grid. Shown are the horizontal (a) and vertical (b) components of the upscaled permeability tensor, as well as the coarse scale pressure

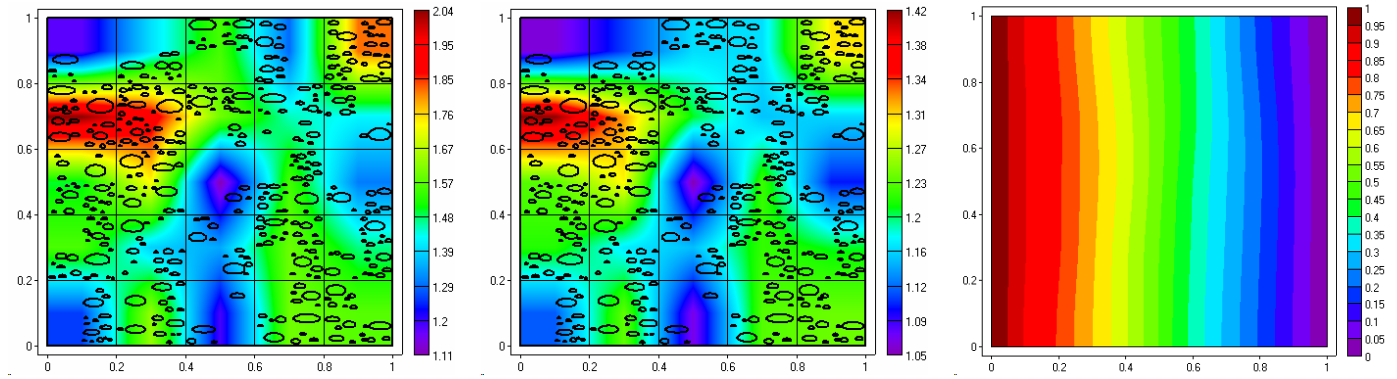

(a) K_{11} (b) K_{22} (c) Coarse-scale pressure

Figure 6: Upscaling results for vugs in homogeneous background permeability field on a 5×5 grid. Shown are the horizontal (a) and vertical (b) components of the upscaled permeability tensor, as well as the coarse scale pressure

Table 1: L_2 errors between coarse-scale pressures and averaged fine-scale pressures on respective coarse grid models

Coarse grid	Constant K		Variable K	
	L_2 error	Relative L_2 error	L_2 error	Relative L_2 error
5×5	1.08×10^{-2}	1.9%	2.16×10^{-2}	3.92%
10×10	6.81×10^{-3}	1.1%	1.18×10^{-2}	2.14%

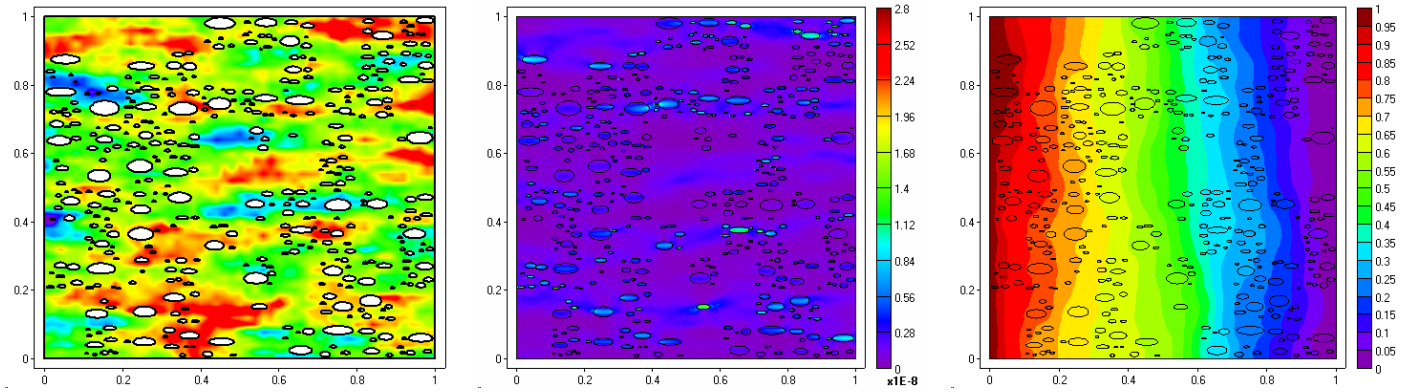

(a) Fine-scale permeability (log plot) (b) Velocity magnitude (c) Pressure

Figure 7: Fine-scale permeability field (a) and reference solution (b,c) for vugs in variable background permeability field. The fine-scale permeability is shown in a log plot. The fine-scale reference solution is shown in (b) and (c).

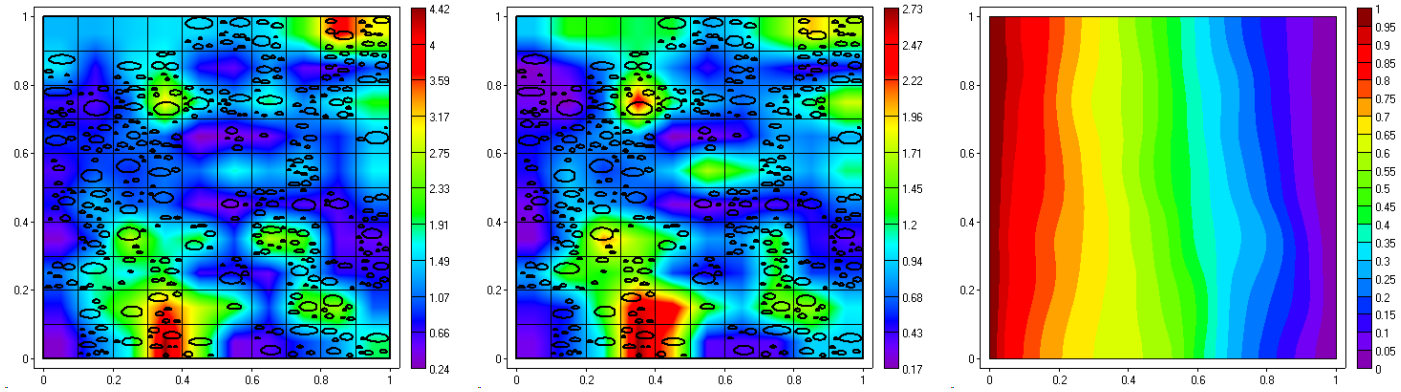

(a) K_{11} (b) K_{22} (c) Coarse-scale pressure

Figure 8: Upscaling results for vugs in heterogeneous background permeability field on a 10×10 grid. Shown are the horizontal (a) and vertical (b) components of the upscaled permeability tensor, as well as the coarse scale pressure

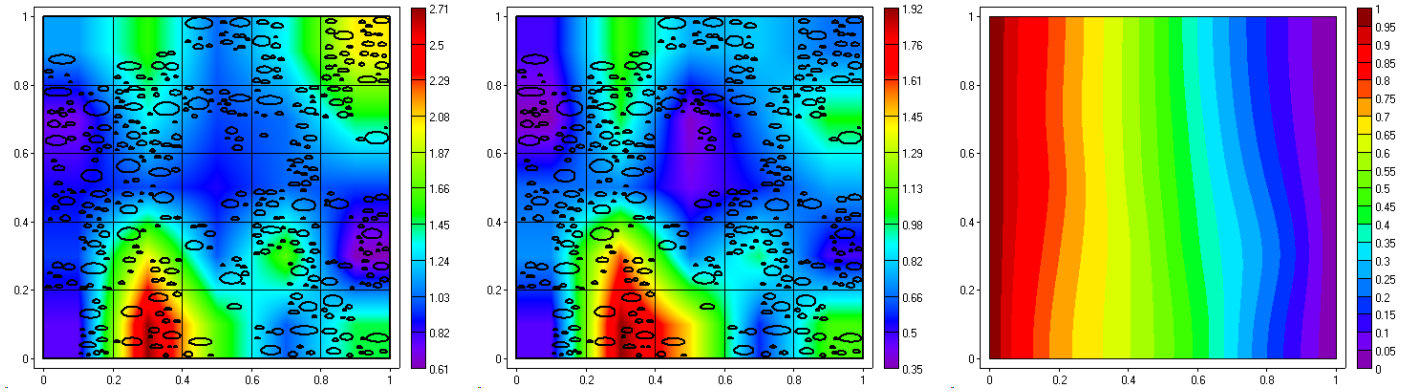

(a) K_{11} (b) K_{22} (c) Coarse-scale pressure

Figure 9: Upscaling results for vugs in heterogeneous background permeability field on a 5×5 grid. Shown are the horizontal (a) and vertical (b) components of the upscaled permeability tensor, as well as the coarse scale pressure

Heterogeneous matrix permeability In the next example, we consider a heterogeneous, isotropic background permeability, as shown in Figure 7(a).The vug population (size, shape and locations) are identical to the previous example (Figure 4(a)). The fine scale matrix permeability field is a realization of a stochastic field with prescribed overall variance (quantified via σ^2, the variance of $log(k)$), correlation structure and covariance model. It was generated using the GSLIB algorithms, characterized by a spherical variogram. The field has long correlation length in the horizontal direction (0.4) and smaller in the vertical direction (0.1). The boundary conditions are the same as in the previous example.

The fine-scale velocity and pressures fields are plotted in Figures 7(b) and 7(c), respectively. We see from this figure that the heterogeneous permeability creates additional high flow channels for the vugs which enhances the connectivity of the media. This is more evident if one compares Figure 4(b) and Figure 7(b). The longer horizontal correlation length in the background permeability creates several high flow channels in the horizontal direction. The upscaling was performed on the same 10×10 and 5×5 coarse grids as in the previous example. Comparing Figures 8 and 9 with Figures 5 and 6, we can observe that the upscale permeabilities are quite different for homogeneous and heterogeneous background permeabilities. Again, if we compare Figure 8 and Figure 9, the results from higher upscaling resolution can more accurately represent the heterogeneity of both vug distribution and background permeability, as also can be seen from Table 1 with L_2 errors in both cases less than 4%.

These tests suggest that the proposed upscaling method provides accurate coarse-scale solution for both homogeneous and heterogeneous background permeability fields. Upscaling resolution has clear effects on the accuracy of upscaling results. Higher resolution can better represent the fine scale heterogeneity and thus gives better results, while it is well expected that higher resolution also requires more computational resources.

Case studies from Tahe oil field

Large aperture, long-range cave In this example we study the effective response of a coarse block of dimensions $50 \times 50m$ with a large aperture cave. The geometry is shown in Figure 10(a). Geological data indicates that the cave has a large aperture (several meters). Well test data indicates that the effective permeability of such coarse blocks is in the order of $100mD$. Due to the large aperture of the cave, the measured effective permeability suggests that some kind of filling material is present in the cave.

Next, we perform a parameter study aimed at determining the properties of the fill-in material. The basic idea is to compute the effective permeability of the entire block for a number of values of K_f. In this way we can obtain a tabulated functional dependence of the upscaled permeability on the fracture permeability. The permeability of the rock has a known value of $K_R = 0.025mD$. The nature of the fill-in material is not well understood, so we vary the permeability of the fracture K_f from $0.025mD$ (effectively a completely blocked cave) to infinity (completely unobstructed Stokes flow) by computing the effective permeability for a range of values for K_f.

The results are shown in Figure 11. Based on these results, it can be seen that an effective permeability of $100mD$ for the entire block results from a fracture permeability of about $1D$. This implies that the fill-in material has the permeability of, for example, fine sand [26]. The velocity field for fracture permeability of $1D$ is shown in Figure 12(a). Note that in the Stokes limit ($k_f \to \infty$) the permeability of such large aperture caves is in the order of $10^{14} - 10^{15}mD$. This is not surprising, as a cave of several meters aperture can easily support fluid velocities in the meters-per-second range (Figure 12(b)).

Large, short-range caves connected by fracture network In this example we study the effective response of a coarse block of dimensions $20 \times 20m$ with five large aperture, short-range caves. The caves are connected by four fractures of approximately $5-30mm$ aperture. The geometry is shown in Figure 13(a). Well test data indicates that the effective permeability of these types of coarse blocks is in the range $10^3 - 5 \times 10^4 mD$. We again perform a parametric study to obtain the dependence of the effective permeability on the fracture permeability.

The permeability of the porous rock matrix has a known value of $K_R = 0.025mD$. The caves are assumed to be fill-in free, that is the flow is completely unobstructed and governed by the Stokes equations. The permeability of the fracture K_f is varied from $0.025mD$ (a completely blocked fracture) to infinity (completely unobstructed Stokes flow). The results are shown in Figure 14. Based on these results, it can be seen that an effective permeability of $1D$ for the entire block (the low end estimate) results from a fracture permeability of about $350D$. The upper limit for effective permeability ($50D$) is achieved for a fracture permeability of approximately $17500D$. Based on typical permeabilities of sand and gravel [26] it can be seen that such overall block permeabilities ($1 - 50D$) can result from well-sorted gravel as the fracture filling material. Moreover, the simulations show that most of the flow occurs in the vug-fracture network. Thus, the overall permeability of such coarse blocks is determined mostly by the aperture and connectivity of the fracture network.

Fracture network in low-permeability rock matrix In this example we study the effective response of a coarse block with an intersecting network of long-range fractures Figure 15(a). Unlike the previous cases, no vugs and caves are present. The fractures have typical aperture of $500 - 1000\mu m$ and spatial density of $2 - 8$ fractures per meter. Well test data indicates that the effective permeability of these types of coarse blocks is in the range $10^3 - 5 \times 10^4 mD$. As in the previous examples we would like to find out the effective permeability of the block as a function of the fracture fill in material.

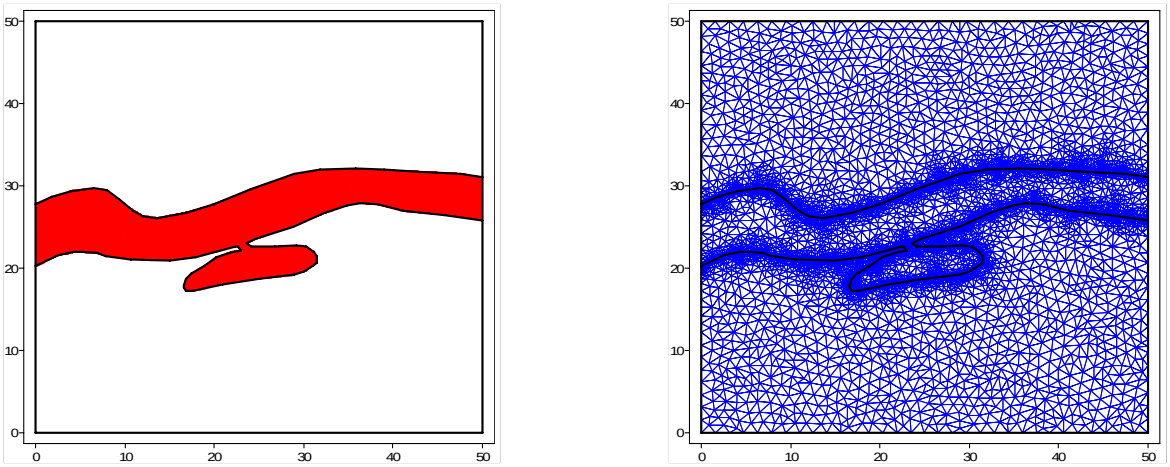

(a) Coarse block (b) Discretization

Figure 10: The coarse block (a) consisting of porous rock and a large cave (red) of approximately $4 - 8m$ aperture, running trough the block. The unstructured mesh used in the computations is shown in (b).

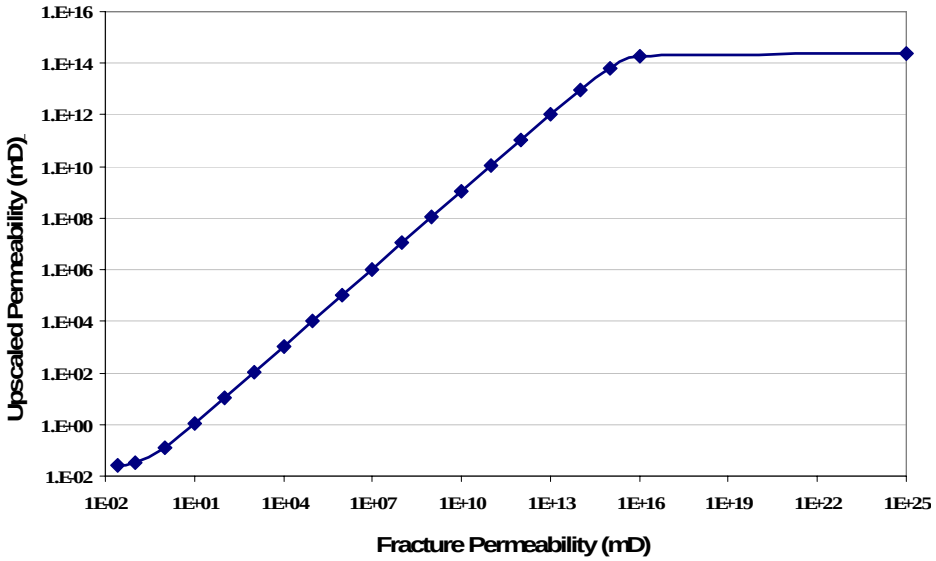

Figure 11: Effective permeability (K_{11}^* component) of the coarse block as a function of the fracture permeability

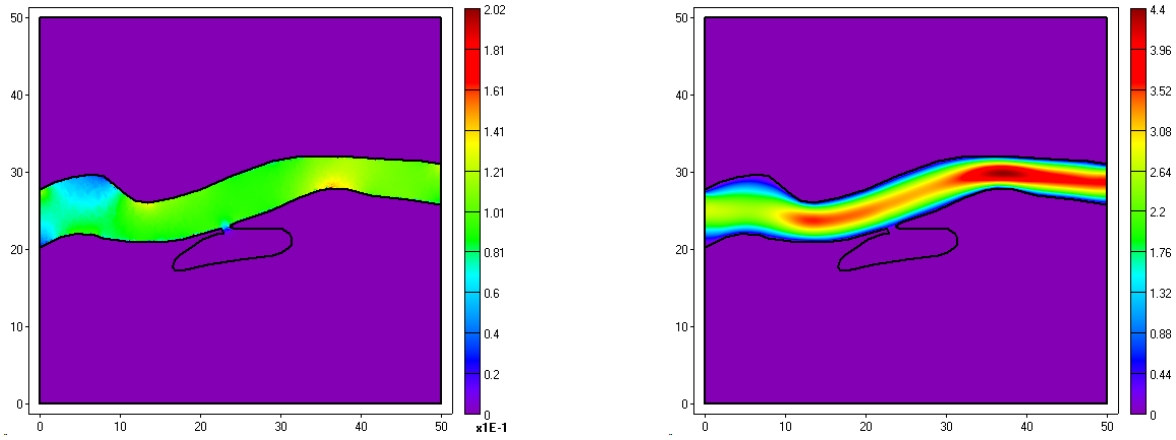

(a) $K_f = 1D$ (b) $K_f = \infty$ (Stokes limit)

Figure 12: Fine-scale velocity field for filling material with permeability of fine sand (a) and the completely unobstructed Stokes limit (b).

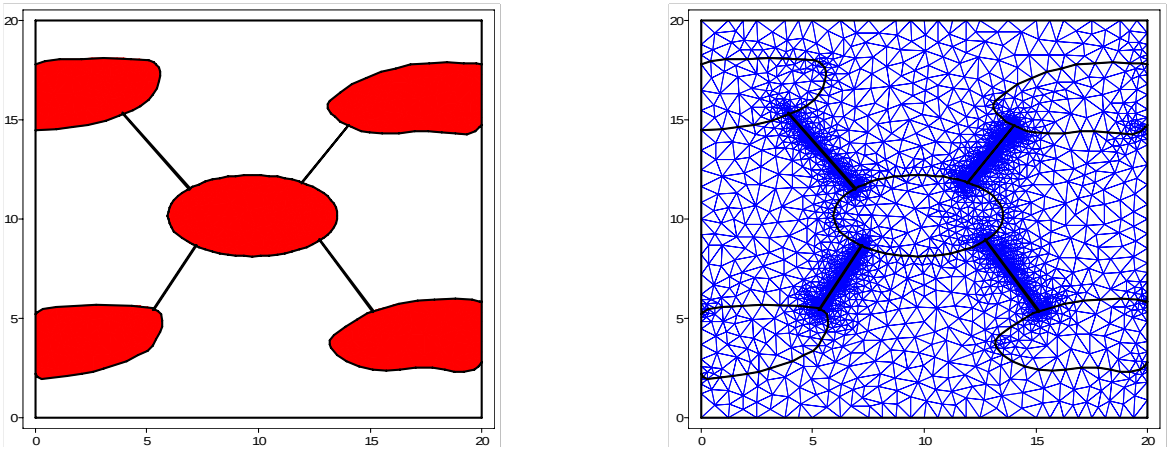

(a) Coarse block (b) Discretization

Figure 13: The coarse block (a) consisting of porous rock and several large, short-range caves (red) of approximately $4-6m$ aperture, connected by fractures (black lines). The unstructured mesh used in the computations is shown in (b).

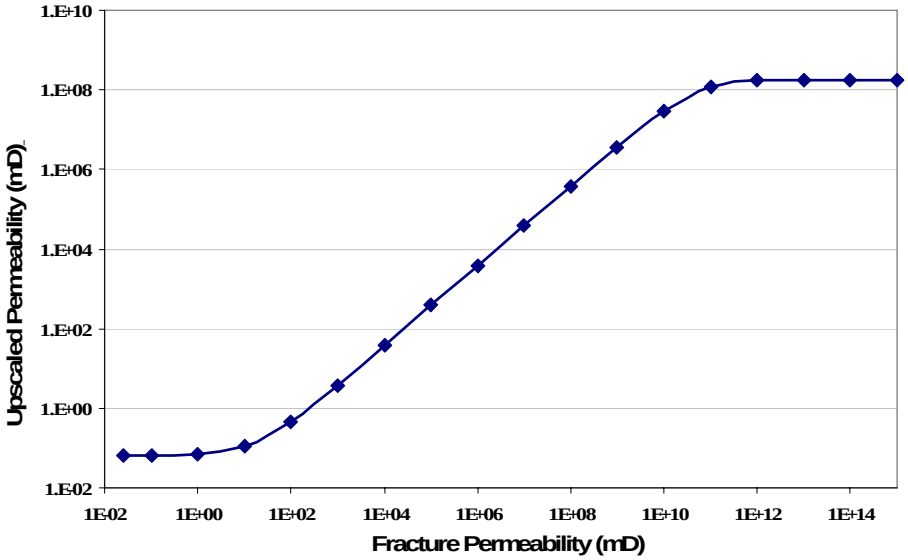

Figure 14: Effective permeability (K^*_{11} component) of the coarse block as a function of the fracture permeability

For the computations, we selected a periodic arrangement of fractures networks as shown in Figure 15(a). Two evenly distributed fracture networks that run at 45 degrees to the coordinate axes and intersect with each other at right angles were used. A uniform fracture aperture of $707\mu m$ was used for all fractures. The spatial density of both networks was selected to be 2.3 fractures per meter. This allowed, using periodicity, to use a relatively small REV of dimensions $0.3 \times 0.3m$ as shown in Figure 15(a). The permeability of the rock matrix is taken to be $K_R = 0.025mD$ (as in the previous sections). The fracture permeability K_f is varied from $0.025mD$ (a completely blocked fracture) to infinity (completely unobstructed Stokes flow).

The results are shown in Figure 16. It can be seen that completely unobstructed fractures (no fill-in) result in effective permeability of $139D$. A $1D$ effective permeability will result (for this particular network of uniform aperture of $707\mu m$ and spatial density of 2.3 fractures per meter) from a fill-in material with permeability $K_f = 364D$. This implies that the filling is well sorted gravel. On the other hand, the upper limit of $50D$ effective permeability the fracture must be nearly unobstructed ($K_f = 4.47 \times 10^4 D$). Note that in this simulation, perfectly smooth fractures of uniform aperture are assumed. Thus, while an unobstructed fracture network yields a $139D$ effective permeability, effects of fracture wall roughness and non-uniform aperture can easily change this effective permeability by an order of magnitude.

In conclusion, note that the effective permeability is influenced not only by the fill-in material but also by the fracture density and fracture aperture. For example a more dense network of fractures of, for example, 8 fractures per meter will result in approximately $480D$ permeability in

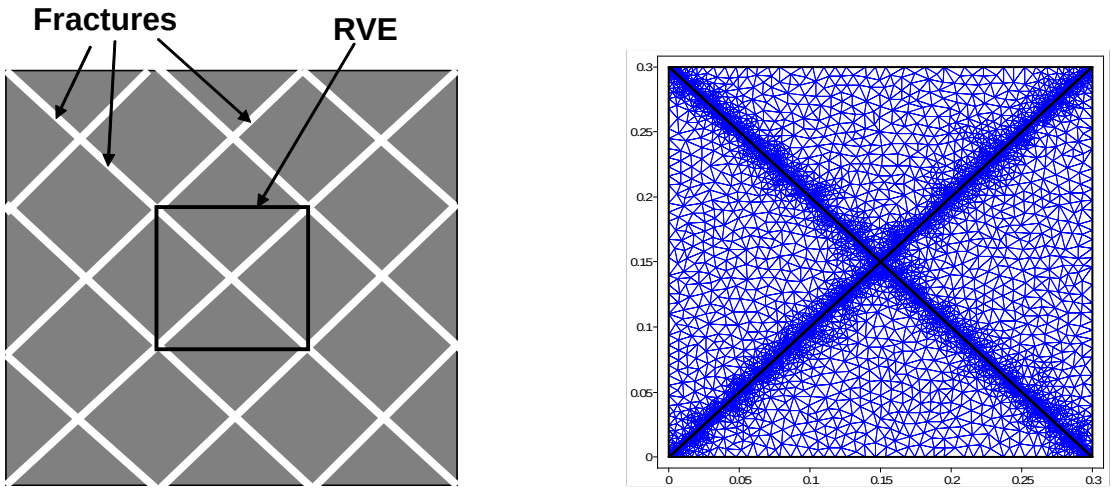

(a) Coarse block (b) Discretization

Figure 15: The coarse block (a) consisting of porous rock (grey region) and intersecting fractures (white strips). Due to the periodic arrangement of the fractures a smaller REV is used in the computations (black rectangle). The unstructured mesh used in the computations is shown in (b).

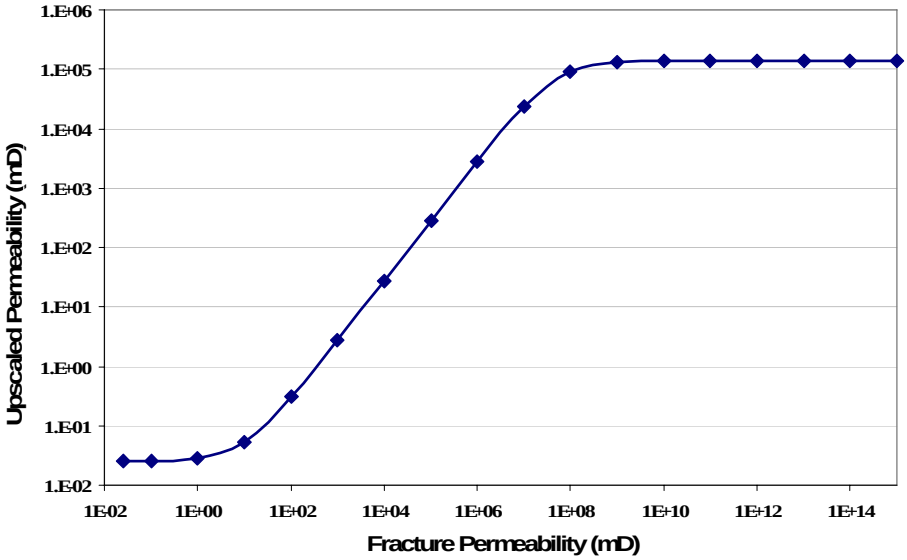

Figure 16: Effective permeability (K^*_{11} component) of the coarse block as a function of the fracture permeability

the Stokes limit (no fill-in). Thus a more detailed characterization of the fracture networks present in Tahe field is needed to better quantify the these types of fracture networks. Alternatively, an expanded parametric study which also includes the fracture density and variable aperture may be performed.

Vugs/Caves imbedded in a fractured matrix In this example we study the interaction between porous rock, vugs and small fractures ($< 1\mu m$) with density in the range $2-8$ fractures per meter. A conceptual picture of such media is shown in Figure 17(a). Note that the fractures are not drawn to scale (they are much thinner than they appear in the figure) and their density (number of fracture per meter in some direction) may vary. Again we are interested in the effective response of a typical coarse block.

We are considering a coarse block of dimension $20 \times 20m$. The fracture network imposed on the porous matrix is of aperture $707\mu m$ and density 2.3 fractures per meter. Geometrically this is equivalent to the fractured porous rock of the previous section. The same permeability of the porous rock ($0.025mD$) as previously is used. Two elliptically shaped vugs of dimension $3.8 \times 5.2m$ are imbedded in this fractured rock. Note that for a $20 \times 20m$ bock the fracture density of 2.3 implies that we have around 12 fractures in each direction (the fractures are at 45 degrees to the coordinate axes).

The very small aperture of the fractures compared to the block dimension (the ratio is approximately 1 : 28000) makes a direct numerical simulation of the porous

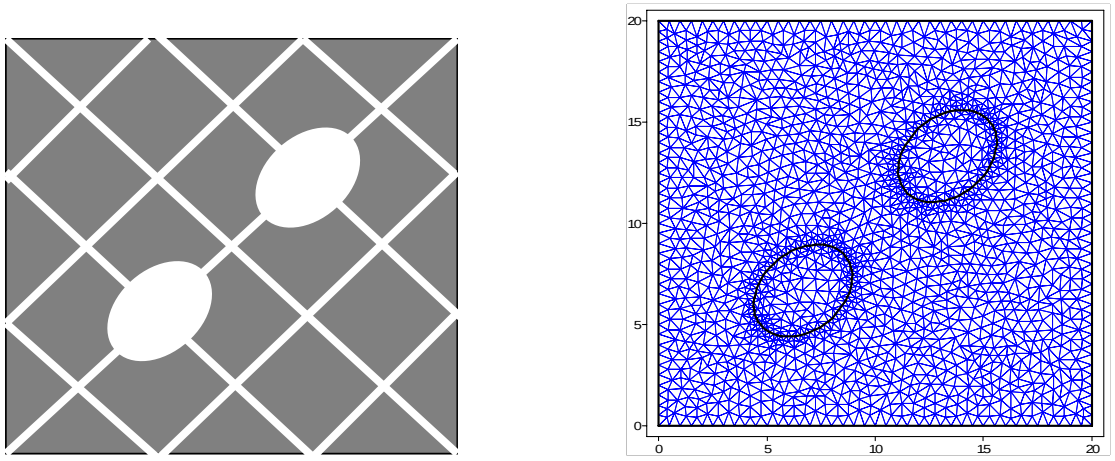

(a) Coarse block (b) Discretization

Figure 17: The coarse block (a) consists of fractured porous rock and two imbedded elliptical vugs. The porous rock is the grey region and the fractures are conceptually depicted as white strips. The fractures are not drawn to scale - the block is of dimension $20 \times 20m$ and the fracture thickness is much smaller ($707\mu m$) than depicted. The very small size of the fractures makes impossible a direct simulation, so a two scale homogenization approach is used. The unstructured mesh used in the second homogenization step is shown in (b).

rock/fractures/vug system very difficult. Thus we used a two-stage homogenization approach. First, we consider the porous rock and the fractures alone and replace it with an equivalent effective homogeneous porous medium which we call matrix. The permeability of this medium is denoted by K_m. Next we imbed the two vugs in this effective medium and homogenize again to obtain the final effective permeability of the coarse block

This approach is computationally feasible since the first step involves much smaller REVs. One can take advantage of the periodic arrangement of the fractures and needs to consider only two intersecting fractures (Figure 15(b)), as this was done in the previous section. In the second step one is faced with solving the Stokes-Brinkman equation for the matrix and the imbedded vugs which poses no problems as the vugs are of size similar to the coarse block dimensions.

This approach allows us to use the parametric study developed for fractured rock (Figure 16) to directly compute the final effective coarse permeability. For example, it was found in the previous section, that if our fracture network has permeability of $K_f = 364D$ (due to some fill-in material such as sorted gravel) the effective matrix permeability (porous rock and fractures) is $K_m = 1D$. With this parameters for the fracture network the second homogenization step yields an effective permeability tensor given in table 2. Similarly, it was found that a $K_f = 4.47 \times 10^4 D$ for the fracture network results in effective permeability of $K_m = 50D$ and an unobstructed fracture network results in $K_m = 139D$. The results of the second homogenization step are summarized in table 2. Some selected cell solutions of the second homogenization step are shown in Figures 18- 20.

The use of the two-stage homogenization process (table 2) not only allows us to save computational resources but also to evaluate the influence of the fractures and vugs on the overall effective permeability. The first homogenization step shows orders of magnitude increase in the effective permeability K_m of the ensemble of porous rock and fracture network over the very low permeability of the porous rock itself ($K_r = 0.025mD$). The second homogenization step - the addition of the two vugs further increases the effective permeability (now of the entire ensemble of porous rock, fractures and vugs) by $16 - 18\%$. Thus, the most important contribution to overall permeability is that of the fracture network. This is similar to the result of [27] which concluded that the computed equivalent permeabilities are more sensitive to fracture patterns

Table 2: Effective permeabilities (two-stage homogenization) for coarse block with vugs imbedded in porous, fractured rock.

Fracture permeability	$K_f = 364D$	$K_f = 44755D$	$K_f = \infty$
Homogenization, first step (porous rock and fractures only)	$K_m = 1D$	$K_m = 50D$	$K_m = 139D$
Effective permeability of coarse block (Homogenization, second step)	$\begin{pmatrix} 1.18 & 0.036 \\ 0.036 & 1.18 \end{pmatrix} D$	$\begin{pmatrix} 58.7 & 1.83 \\ 1.83 & 58.7 \end{pmatrix} D$	$\begin{pmatrix} 163.4 & 5.08 \\ 5.08 & 163.4 \end{pmatrix} D$

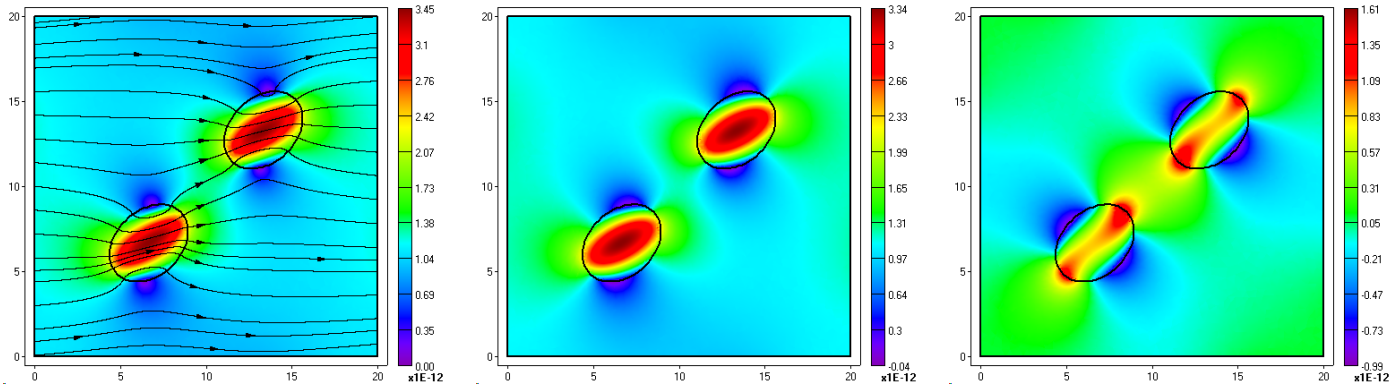

(a) Velocity magnitude and streamline (b) Horizontal component (v_1) (c) Vertical component (v_2)

Figure 18: Second stage homogenization cell solution used to determine K_{11} and K_{21} for the case of matrix permeability of $K_m = 1D$. This corresponds to a fracture permeability of $K_f = 364D$ at the finer scale (See Figure 16). Shown are velocity magnitude and streamlines (a), horizontal velocity component (b) and vertical velocity component (c).

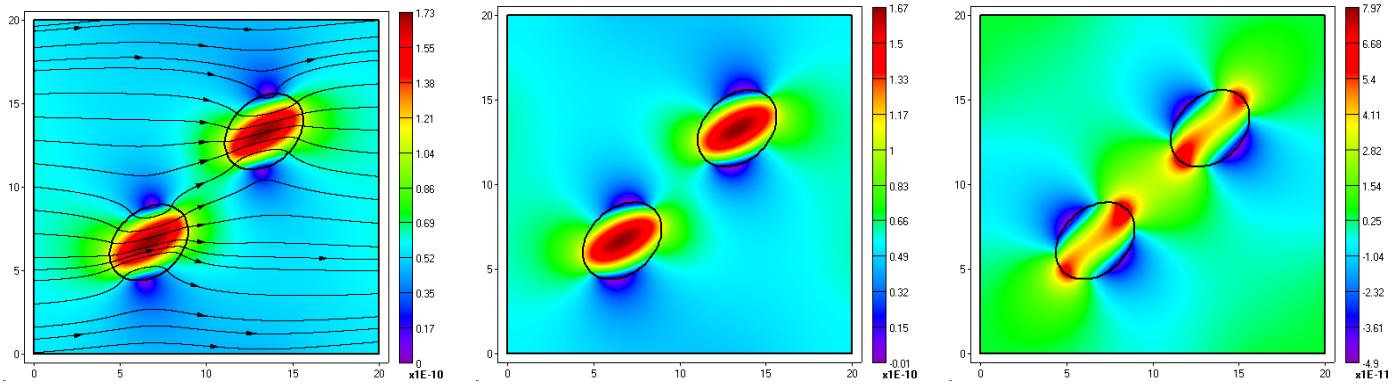

(a) Velocity magnitude and streamline (b) Horizontal component (v_1) (c) Vertical component (v_2)

Figure 19: Second stage homogenization cell solution used to determine K_{11} and K_{21} for the case of matrix permeability of $K_m = 50D$. This corresponds to a fracture permeability of $K_f = 44755D$ at the finer scale (See Figure 16). Shown are velocity magnitude and streamlines (a), horizontal velocity component (b) and vertical velocity component (c).

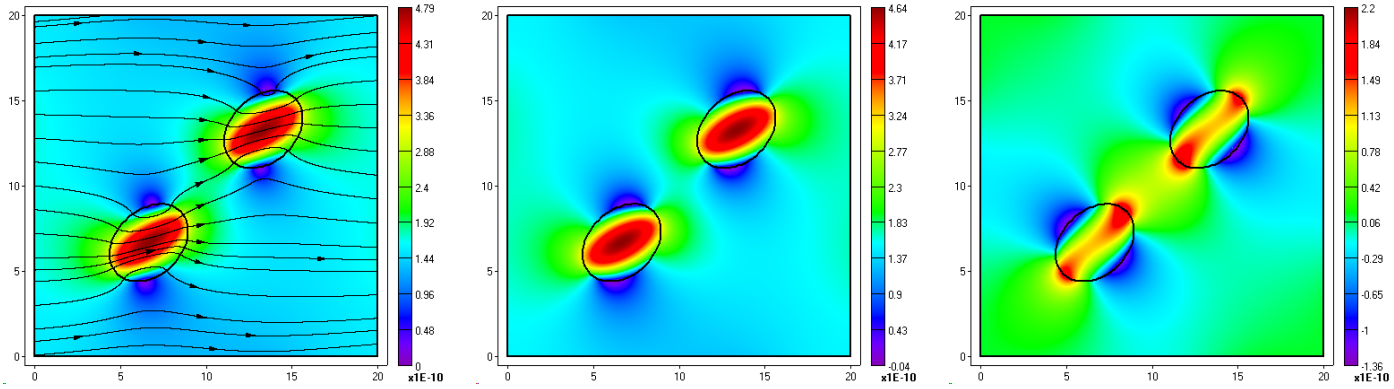

(a) Velocity magnitude and streamline (b) Horizontal component (v_1) (c) Vertical component (v_2)

Figure 20: Second stage homogenization cell solution used to determine K_{11} and K_{21} for the case of matrix permeability of $K_m = 139D$. This corresponds to completely free-flow fractures at the finer scale (See Figure 16). Shown are velocity magnitude and streamlines (a), horizontal velocity component (b) and vertical velocity component (c).

and connectivity.

It should be noted however the extremely large scale difference between the vugs and the fractures - about $5000:1$ if comparing the characteristic dimensions of the vugs to the fracture aperture. Thus, for all practical purposes, the vugs can be considered as well separated, isolated vugs in an fractured porous rock matrix. The situation however may change drastically if the vugs are closely spaced together, or if there is a high-permeability channel connecting them, as for example was the case in the previous discussion Figure 7.

Conclusions

In this work, we propose using the Stokes-Brinkman equation as a unified approach to model the flow through carbonate karst formations. By properly choosing the coefficients, this model automatically adapts to Stokes equation in free flow regions and Darcy's law in porous rock matrix. It is shown that this model can be upscaled to Darcy law on a coarse scale with standard homogenization procedures.

We evaluated the validity of this model on 2D and 3D problems. In a domain with randomly populated elliptical vugs, we performed upscaling computations by comparing the coarse-scale results with averaged fine-scale solutions. Both homogeneous and heterogeneous background permeabilities were considered. It was shown that the presence of high permeability channels connecting vugs can substantially effect the overall flow pattern. The numerical tests also show that the proposed upscaling to Darcy law at coarse scale is accurate in the case of isolated vugs. The effect of upscaling resolution is investigated by comparing results on 10×10 and 5×5 coarse grids. As expected, higher resolution can better represent the fine scale heterogeneity and thus gives better accuracy.

We performed serval case studies of typical configurations in a oil field in China. We investigate the effects of partial filled fractures on the overall permeability of the coarse block. It is shown that the permeability of the filling materials have profound effect on the coarse scale, especially in the transition regions between Darcy and Stokes regions. It is difficult for the traditional coupled Darcy-Stokes method to model the flow in such regions. Sensitivity studies are carried out based on the proposed Stokes-Brinkman equation. It is demonstrated that if we know the overall permeability of the coarse block (say from well testing analysis), we can estimate the filling materials' permeability the and thus determine their possible rock type.

Nomenclature

$\mathbf{D}$ = fluid strain rate

f = source term

$\mathbf{K} = \begin{pmatrix} \mathbf{K}_{11} & \mathbf{K}_{12} \\ \mathbf{K}_{21} & \mathbf{K}_{22} \end{pmatrix}$ permeability (md)

l = characteristic length of fine scale

L = characteristic length of coarse scale

L_2 = the standard norm for square-integrable functions

$\mathbf{n}$ = unit normal of interface between vugs and rock matrix

p = pressure (Pa)

$\mathbf{v}$ = velocity (m/s)

α_{BJ} = coefficient in Beavers-Joseph tye interface conditions

ϵ = small parameter (l/L)

σ = fluid stress tensor

μ = fluid physical viscosity (cp)

μ^* = effective viscosity in Stokes-Brinkman equation (cp)

Acknowledgements

This paper is dedicated to Dr. Richard Ewing for his help and leadership. Financial support from SINOPEC is gratefully acknowledged.

References

1. Hornung, U.: *Homogenization and porous media*, Interdisciplinary Applied Mathematics. 6.New York, Springer (1997).
2. Beavers, G. and Joseph, D.: "Boundary Conditions at a Naturally Permeable Wall," (1967) **30**, 197.
3. Saffman, P.: "On the boundary condition at the surface of a porous medium." *Studies appl. Math.* (1971) **50**, 93.
4. Sanchez-Palencia, E. and Ene, H.: "Equations et phénomènes de surface pour l'écoulement dans un modèle de milieu poreux," *Journal de Mécanique* (1975) **14**, 73.
5. Levy, T. and Sánchez-Palencia, E.: "On boundary conditions for fluid flow in porous media," *Internat. J. Engrg. Sci.* (1975) **13**, 923.
6. Sanchez-Palencia, E.: *Non-Homogeneous Media and Vibration Theory*, volume 127 of *Lecture Notes in Physics*, Springer-Verlag, Berlin (1980).
7. Kaviany, M.: *Principles of Heat Transfer in Porous Media*, Mechanical Engineering Series, Springer-Verlag, New York (1999).
8. Jäger, W. and Mikelić, A.: "On the boundary conditions at the contact interface between a porous medium and a free fluid," *Ann. Scuola Norm. Sup. Pisa Cl. Sci. (4)* (1996) **23**, 403.
9. Jäger, W. and Mikelić, A.: "On the interface boundary condition of Beavers, Joseph, and Saffman," *SIAM J. Appl. Math.* (2000) **60**, 1111.
10. Jaeger, W., Mikelic, A. and Neuss, N.: "Asymptotic analysis of the laminar viscous flow over a porous bed," *SIAM J. Sci. Comput.* (2001) **22**, 2006.
11. Arbogast, T. and Lehr, H.L.: "Homogenization of a Darcy-Stokes system modeling vuggy porous media," *Comput. Geosci.* (2006) **10**, 291.
12. Darcy, H.: *Les fontaines publique de la ville de Dijon*, Librairie des Corps Impériaux des Ponts et Chaussées et des Mines, Paris (1856).
13. Laptev, V.: *Numerical solution of coupled flow in plain and porous media*, Ph.D. thesis, Technical University of Kaiserslautern, Germany (2003).

14. Brinkman, H.C.: "A Calculation of the Viscous Force Exerted by a Flowing Fluid on a Dense Swarm of Particles," *Applied Scientific Research Section A-Mechanics Heat Chemical Engineering Mathematical Methods* (1947) **1**, 27.
15. Lundgren, T.S.: "Slow flow through stationary random beds and suspensions of spheres," *Journal of Fluid Mechanics* (1972) **51**, 273.
16. Neale, G. and Nader, W.: "Practical Significance of Brinkmans Extension of Darcys Law - Coupled Parallel Flows Within a Channel and a Bounding Porous-Medium," *Canadian Journal of Chemical Engineering* (1974) **52**, 475.
17. Koplik, J., Levine, H. and Zee, A.: "Viscosity renormalization in the Brinkman equation," *Physics of Fluids* (oct 1983) **26**, 2864.
18. Allaire, G.: "Homogenization of the Navier-Stokes equations and derivation of Brinkman's law," *Mathématiques appliquées aux sciences de l'ingénieur (Santiago, 1989)*, Cépaduès, Toulouse (1991) 7–20.
19. Martys, N., Bentz, D.P. and Garboczi, E.J.: "Computer simulation study of the effective viscosity in Brinkman's equation," *Physics of Fluids* (apr 1994) **6**, 1434.
20. Zhikov, V., Kozlov, S. and Oleinik, O.: *Homogenization of Differential Operators and Integral Functionals*, Springer-Verlag, Berlin (1994).
21. Sahraoui, M. and Kaviany, M.: "Slip and no-slip velocity boundary conditions at interface of porous, plain media," *International Journal of Heat and Mass Transfer* (1992) **35**, 927.
22. Ene, H.: "Application of the Homogenization Method to Transport in Porous Media," *Dynamics of Fluids in Hierarchical Porous Media*, ed. J. Cushman, Academic Press, London (1990) 223–241.
23. Turek, S.: *Efficient Solvers for Incompressible Flow Problems: An Algorithmic and Computational Approach*, Springer Verlag, New York (1999).
24. Burman, E. and Hansbo, P.: "A unified stabilized method for Stokes' and Darcy's equations," *Journal of Computational and Applied Mathematics* (2007) **198**, 35.
25. Ciarlet, P.: *The Finite Element Method for Elliptic Problems*, number 40 in Classics in Applied Mathematics, SIAM, Philadelphia (2002).
26. Bear, J.: *Dynamics of Fluids in Porous Media*, Dover, New York (1972).
27. Philip, Z. *et al.*: "Modeling coupled fracture-matrix fluid flow in geomechanically simulated fracture networks," *SPE Reservoir Evaluation & Engineering* (2005) **8**, 300.